Coexistence of a two- and three-dimensional Landau states in a wide parabolic quantum well

C. S. Sergio,* G. M. Gusev, and J. R. Leite
Instituto de Física da Universidade de São Paulo, SP, Brazil

E. B. Olshanetskii, A. A. Bykov, N. T. Moshegov, A. K. Bakarov, and A. I. Toropov
Institute of Semiconductor Physics, Novosibirsk, Russia

D. K. Maude and O. Estibals
GHMF, MPI-FKF/CNRS, BP-166, F-38042, Grenoble, Cedex 9, France
and INSA-Toulouse, 31077, Cedex 4, France

J. C. Portal
GHMF, MPI-FKF/CNRS, BP-166, F-38042, Grenoble, Cedex 9, France,
INSA-Toulouse, 31077, Cedex 4, France,
and Institut Universitaire de France, Toulouse, France

(Received 9 January 2001; revised manuscript received 12 April 2001; published 29 August 2001)

Shubnikov–de Haas oscillations are measured in wide parabolic quantum wells with five to eight subbands in a tilted magnetic field. We find two types of oscillations. The oscillations at low magnetic fields are shifted toward higher field with the tilt angle increasing and can be attributed to two-dimensional Landau states. The position of the oscillations of the second type does not change with increasing the tilt angle which points to a three-dimensional character of these Landau states. We calculate the level broadening due to the elastic scattering rate $\Gamma=\hbar/2\tau$, where τ is the quantum time, and the energy separation between two-dimensional subbands, $\Delta_{ij}=E_j-E_i$, in a parabolic well. For all levels we obtain $\Gamma_j\sim\Delta_{ij}$, which means that the levels overlap, supporting the observation of three-dimensional Landau states. Surprisingly, we find that the lowest subband, which has a smaller energy separation from the higher level, does not overlap with these subbands and forms a two-dimensional state.

DOI: 10.1103/PhysRevB.64.115314 PACS number(s): 73.50.Jt, 72.20.My, 71.70.Di, 73.43.−f

I. INTRODUCTION

The existence of an energy gap in the electron spectrum of two-dimensional electron gas in a strong magnetic field is a crucial point for an explanation of the quantum Hall effect (QHE).[1] It demonstrates why the QHE is a property of the two-dimensional (2D) system and is not observed in the three-dimensional case, where the electron spectrum is continuous. However, the evolution of states of a quasi-two-dimensional system toward a three-dimensional system has not been studied yet. It is expected that for a wide quantum well the energy spectrum consists of a Landau level belonging to different electric subbands. In a real system the energy levels have finite widths because of the disorder; therefore, when the corresponding electric subbands and their Landau levels overlap, the electronic system has a 3D energy spectrum, and the QHE should disappear. For a square well the energy spectrum E_i is given by

$$E_i=\frac{i^2(h/w_e)^2}{8m_e}, \tag{1}$$

where m_e is the effective electron mass, i is the subband index, and w_e is the well width. We see that the energy separation increases for higher levels with subband number. Therefore, it is expected that the lower 2D levels would be the first to overlap when the quantum well width increases.

Experimentally, a quasi-three-dimensional system can be obtained by the growth of epitaxial layers of heavily doped semiconductors with a thickness of the order of 1000–2000 Å. Very recently the quantization of the Hall resistance and the appearance of minima in the diagonal resistance have been observed in a three-dimensional disordered GaAs film.[2] Because of strong disorder, the samples demonstrated a three-dimensional behavior of the Shubnikov–de Haas (SdH) oscillations. It has been assumed that the Coulomb gap due to electron-electron interactions occurs at a high magnetic field and leads to deep minima in the longitudinal and quantization of the diagonal conductivity components. However, further experimental and theoretical works are necessary to clarify the effect of the electron-electron interaction on single-electron gaps in the wide quantum well. Another remarkable example of the quasi-three-dimensional system is a parabolic quantum well (PQW).[3] The basic idea behind these structures is to create a conduction band profile in the growth direction of GaAs/AlGaAs heterostructures by properly varying the Al mole fraction such that it mimics the parabolic potential of a uniformly distributed slab of positive charge. It allows one to form a wide layer of highly mobile carriers with uniform density. Considerably larger mobility in comparison with heavily doped GaAs epitaxial layers has been achieved by removing the dopant atoms from the quantum well. Many experimental results in the case of two occupied subbands have been obtained in such structures.[4] In samples with a

2000 Å well width a quasi-two-dimensional system with four occupied subbands has been realized.[5] Low-field SdH oscillations demonstrated the existence of several subbands with different densities. Although tilted magnetic field measurements have not been performed, the behavior of the SdH oscillations points to a 2D character of the spectrum.

Realization of a dilute high-mobility 3D electron gas in a parabolic quantum well would be promising for the search for electronic-correlated phases predicted in three-dimensional metals in a strong magnetic field.[6] However, the possibility of the realization of a really homogeneous 3D system in a realistic parabolic well may be questioned. Assuming that the quantum mobility is of the order of 100×10^3 cm^2/V s, we obtain that the elastic level broadening $\Gamma = \hbar/2\tau \sim 0.08$ meV. It becomes comparable to the distance between the highest levels only for a 10 000 Å parabolic well, which is difficult to grow. In samples with lower mobility correlated phases are destroyed by impurities. Therefore in a parabolic well with a high mobility and a width smaller than 10 000 Å we expect to find the coexistence of the 2D state belonging to the *highest subband* and 3D states.

However, in a parabolic well it is possible to create a reverse situation—the coexistence of the 2D state belonging to the *lowest subband* and 3D states. This situation is less trivial, because it allows one to compare the transport properties of 2D and 3D electrons with almost the same Fermi energy under the same experimental conditions. As is argued in Ref. 7, the dominant scattering mechanism in a wide parabolic well is the scattering on background ionized impurities. Remote impurity scattering does not appear to have a strong effect in a wide well, because the distance between the dopant layer and the edges of the electron layer is >500 Å for partially full parabolic wells.[5]

In the present work we study 2000 Å and 4000 Å parabolic wells with a narrow (100 Å) spacer and five to eight occupied subbands. Our samples are overfilled, and the width of the electron slab is almost coincident with the geometrical width. Therefore, it is expected that in the sample with a narrow spacer remote impurity scattering would result in a decrease of the electron mobility of the electrons which occupy the higher levels, because the peaks of the wave function are located close to the impurities. The peaks of the wave function for the lowest subband are removed from the effective edge and impurities by $\sim$200–300 Å, which is larger than for the higher levels. Thus the mobility of the electrons in parabolic wells strongly depends on the index number and is greater in the lower subband. Therefore we can expect that the lowest subband does not lose its 2D structure even in a wide quantum well. In order to characterize the wide parabolic well and determine the subband structure we measure the SdH oscillations in a tilted magnetic field. The oscillations contain two frequencies: one depends on the tilt angle, and the other does not. We observe 2D states belonging to the lowest subband, which has smaller energy separation from the higher level for quantum well width $W \leqslant 4000$ Å.

II. EXPERIMENTAL RESULTS

The samples used are the GaAs/Al$_x$Ga$_{1-x}$As PQW grown by molecular-beam epitaxy. On the top of the semi-insulating substrate there is a 1000-nm GaAs buffer layer with 20 periods of AlAs(5 ML)GaAs(10 ML) superlattice, followed by 500 nm Al$_x$Ga$_{1-x}$As with x varying from 0.07 to 0.27, 10 nm Al$_{0.3}$Ga$_{0.7}$As with δ-Si doping, Al$_{0.3}$Ga$_{0.7}$As undoped layer (spacer), and the wide parabolic well. The well is characterized by three parameters: the height of the parabola Δ_1, the width of the parabola W, and the height of the AlGaAs barrier Δ_2.

Two structures have been studied, labeled for convenience A and B. The main difference between these structures is that the parabolic well A has $W = 2000$ Å, $\Delta_1 = 150$ meV, and $\Delta_2 = 120$ meV, and sample B has $W = 4000$ Å, $\Delta_1 = 240$ meV, and $\Delta_2 = 10$ meV. It leads to a small difference in the electron density for a full well: sample A has concentration $n_s = 3.9 \times 10^{11}$ cm^{-2}, and for sample B the concentration is $n_s = 3.5 \times 10^{11}$ cm^{-2}. The parabolic well is full when the electron density in the well n_s is sufficient to completely screen the fictitious positive charge N^+: $n_s = N^+ W = (2\Delta_1 \varepsilon)/(e^2 \pi W)$, where $\varepsilon = 12.87$ is the static dielectric constant. However, the effective bulk density $N^+ = N_{\text{bulk}}$ and Fermi energy E_F for these two samples were different: sample A has $N_{\text{bulk}} = 2.1 \times 10^{16}$ cm^{-3}, $E_F = 3.6$ meV, and sample B has $N_{\text{bulk}} = 8.8 \times 10^{15}$ cm^{-3}, $E_F = 2.05$ meV (for the electron effective mass $m = 0.075\, m_e$).

After the growth the PQW substrate was processed into a Hall bar. Four-terminal resistance and Hall measurements were made down to 30 mK in a magnetic field up to 17 T. The distance between the voltage probes was 250 μm; the width of the bar was 100 μm. The measurements were performed with an ac current not exceeding 10^{-8} A. Resistance was measured for different angles between the field and substrate plane in the magnetic field using an *in situ* rotation of the sample.

For a full parabolic well the sample layer width is close to the geometrical width of the well; therefore, the energy spectrum E_i of a parabolic well can be roughly approximated by the spectrum of a square well given by Eq. (1). We also perform numerical self-consistent calculations for the parabolic well with a width of 2000 Å, which yields five electronic subbands occupied. The mobility of the electron gas in the well is 65×10^3 cm^2/V s. Self-consistent calculations for a parabolic well with a width of 4000 Å show that there are eight occupied subbands. The mobility of the electron gas in this sample is 210×10^3 cm^2/V s for a full well.

Figure 1 shows the low-field dependence of the SdH oscillations for different angles between the magnetic field and the normal to the substrate surface θ. The oscillations are periodic in $1/B$ and have only one frequency. The positions of the oscillations are shifted, as expected for a 2D electron gas, when the magnetic field is tilted from the normal to the substrate. For a 4000-Å parabolic quantum well [Fig. 1(b)] we also observe a suppression of the amplitude of the SdH oscillations. The magnetoresistance is very well described by the conventional formula for the envelope function of the SdH oscillations in the 2D case:[8]

$$\frac{R_{xx} - R_0}{R_0} = 4 \frac{A_T}{\sinh A_T} \exp\left(-\frac{\pi}{\omega_c \tau}\right) \cos\left(\frac{2\pi E_{F(2D)}}{\hbar \omega_c} - \pi\right), \tag{2}$$

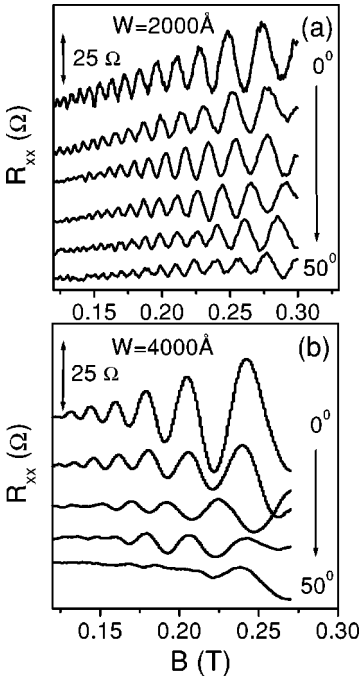

FIG. 1. Low-field part of the magnetoresistance oscillations as a function of the magnetic field, for different angles θ between the applied magnetic field and the normal to the substrate, $T=50$ mK, (a) 2000-Å and (b) 4000-Å parabolic wells.

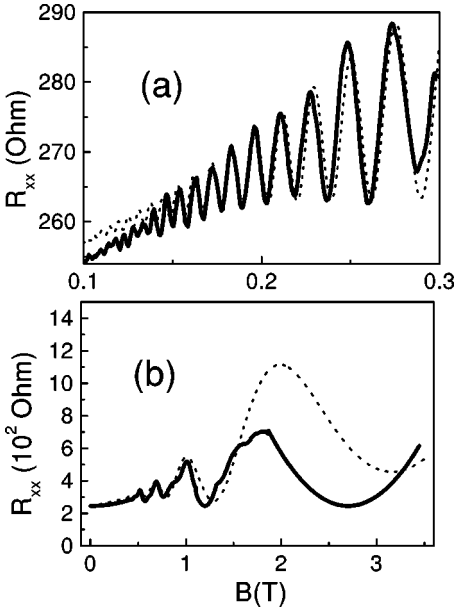

FIG. 2. (a) Low-field magnetoresistance oscillations as a function of the magnetic field at $T=50$ mK, $W=2000$ Å. Solid lines, experimental curves; dashed lines, Eq. (2). (b) Three-dimensional Shubnikov–de Haas (SdH) oscillations obtained by subtraction of the 2D SdH oscillations (a) from the experimental curve (Fig. 3) in a perpendicular magnetic field at $T=50$ mK. Dashed lines, Eq. (3).

where $A_T=(2\pi^2 k_B T)/(\hbar\omega_c)$, $\omega_c=(eB)/(mc)$ is the cyclotron frequency, m is the electron effective mass, τ is the single-particle relaxation time (or quantum time), $E_{F(2D)}$ is the Fermi energy for the 2D levels, and R_0 represents the classical resistance in zero magnetic field.

Figure 2(a) shows R_{xx} versus B for sample A measured in a perpendicular magnetic field and calculated from expression (2). Since R_{xx} varies only slightly with magnetic field, we perform a polynomial fit to $R_{xx}(B)$. We can see that the position of the peak is not perfectly described by the theoretical expression, and the electron concentration varies with magnetic field. We attribute such behavior to the influence of the higher subbands. The numerical calculations of the energy spectrum of a wide parabolic well in a strong magnetic field[9] demonstrated that the Hartree term and the exchange-correlation terms should be included in the bare well potential. These terms lead to oscillations at the bottom of the well and change the potential height in magnetic field. Therefore the electron-electron interaction terms in such a system are as important as external potentials in the Schrödinger equation. Depopulation of the Landau levels of the highest subbands induces a change in the potential well shape and a redistribution of the carriers between subbands. From comparison of the experimental SdH oscillations and expression (2) we extract the carrier density $n_{s1}=1.4\times10^{11}$ cm^{-2} for sample A and $n_{s1}=0.6\times10^{11}$ cm^{-2} for sample B, which is coincident with the 2D electron density obtained from the calculation for the lowest subband in 2000-Å and 4000-Å parabolic wells. From the Hall effect at low field we obtain $n_s=3.9\times10^{11}$ cm^{-2} for sample A and $n_s=3.4\times10^{11}$ cm^{-2} for sample B. Surprisingly, at this magnetic field we do not see any contribution from the second subband, although the electron density in this subband, for example, is only 20% smaller than the density of the first level. In our attempt to fit theory to the experimental curves, we assume that the single-particle relaxation time τ of the electrons from the second subband is smaller than that of the first subband. However, even for the times ratio $\tau_1/\tau_2=5$ we do not obtain any agreement with experiment at higher magnetic fields. At $B>0.5$ T we observe new SdH oscillations which cannot be described by the conventional expression for 2D electron gas.

Figure 3 shows the experimental dependences $R_{xx}(B)$ for 2000-Å and 4000-Å parabolic wells extended to magnetic fields up to 3 T. We can see four oscillations indicated by vertical lines. The position of these oscillations does not depend on the tilt angle. We attribute such behavior to the formation of three-dimensional Landau states. In a real system the energy levels will have finite width because of the disorder; therefore, corresponding electric subbands can overlap. Naively, it may be expected that the lowest subbands will overlap first, when the width of the well increases, because the distance between the levels, $\Delta_{ij}=E_j-E_i$, increases as the square of the index number. However, if the broadening of the levels Γ_j increases faster than Δ_{ij}, the situation is reversed, and the highest electric subbands merge into a bulk Landau state before the lowest. Therefore, the specific feature of the investigated wide parabolic quantum well is the coexistence of 3D and 2D electron states in the well. In a tilted field the 2D SdH oscillations are shifted to higher magnetic fields [see, for example, peak A in Figs. 3(a) and 3(b)], and can cross the 3D SdH peaks, which do not depend on the tilt angle.

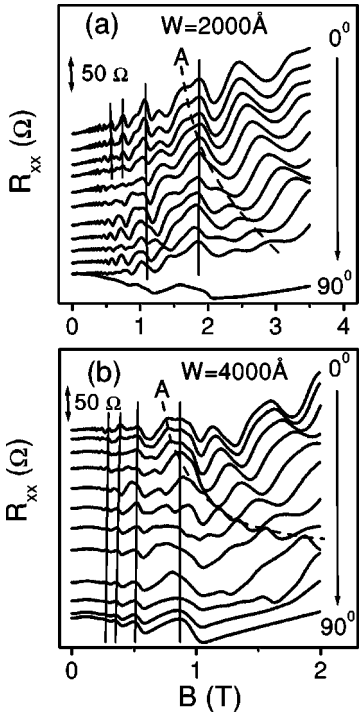

FIG. 3. The magnetoresistance oscillations as a function of the magnetic field up to 3 T for different angles θ between the applied magnetic field and the normal to the substrate, $T=50$ mK, (a) 2000-Å and (b) 4000-Å parabolic wells. Vertical lines, position of the 3D Landau levels. Line A – position of one 2D Landau level which intersects a 3D Landau level in tilted magnetic field.

We subtract the magnetoresistance oscillations of the first subband from the $R_{xx}(B)$ curve at perpendicular magnetic field for a 2000-Å parabolic well. Figure 2(b) shows the results of such subtraction for sample A. The theoretical expression for the SdH oscillations in the 3D case is slightly different from the 2D case:

$$\frac{\Delta R_{xx}}{R_0}=\frac{2}{5}\left(\frac{\hbar\omega_c}{2E_{F(3D)}}\right)^{1/2}\frac{A_T}{\sinh A_T}\times\exp\left(-\frac{\pi}{\omega_c\tau}\right)\cos\left(\frac{2\pi E_{F(3D)}}{\hbar\omega_c}-\frac{\pi}{4}\right), \qquad (3)$$

where $E_{F(3D)}$ is the Fermi energy of the 3D state. Figure 2(b) also shows the plot of the longitudinal resistance versus B calculated from Eq. (3). We can see that the last peak does not fit very well with the experimental curve. We assume that this peak is a spin-down split peak of the last 3D Landau level. In this case we attribute this deviation from $1/B$ periodicity to the formation of two-dimensional electron Landau levels from the last spin-up split 3D level in the quantum Hall effect regime. For sample A, the fits of Eq. (3) to the experimental curve with 3D SdH oscillations give a value of the Fermi energy of $E_{F(3D)}=3.24$ meV. From this value we find the bulk concentration for the higher subbands, $N^*=1.7\times10^{16}$ cm^{-3}. The density profile for the four higher subbands is not a constant and has a deep minimum in the center as we can see in Fig. 4; therefore, the sheet density cannot be recalculated from the equation $n_s=w_eN_{3D}$. The

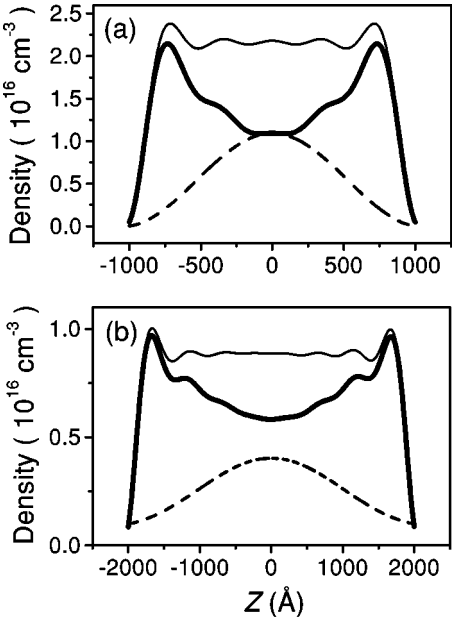

FIG. 4. Electron density profile as a function of position in the well for top subbands (solid line) and bottom subband (dashes), (a) 2000-Å and (b) 4000-Å parabolic wells. The thin solid line, total density profile.

density profile of the lowest subband is sharply peaked (Fig. 4). The width of the self-consistent electron density profiles can be defined as

$$(\Delta z)^2=\frac{12}{n_s}\int_0^W\left(z-\frac{W}{2}\right)^2 n(z)dz, \qquad (4)$$

where $n(z)$ is the electron density profile in the well. It can be expressed as $n(z)=\Sigma n_i|\phi_i(z)|^2$, where n_i is the sheet density in the ith subband, and ϕ_i is the envelope function of the electrons in the ith subband. The sheet density of the electrons in the four higher subbands for sample A is $n_s^*=n_s-n_{s1}=2.5\times10^{11}$ cm^{-2}. We obtain the self-consistent value $\Delta z^*=1200$ Å and find the bulk density for the quasi-three-dimensional subband, $N^*=n_s^*/\Delta z^*=2.05\times10^{16}$ cm^{-3}, which is slightly larger than the bulk density determined from the measurements of the 3D SdH oscillations.

It is worth noting that the positions of the last two peaks of the bulk SdH oscillations remain the same in a parallel magnetic field. The magneto-oscillations in the presence of the in-plane magnetic field are usually called diamagnetic SdH oscillations.[4] At low parallel magnetic field each electron level in the quantum well is the hybrid electric-Landau subband. Low-field levels do not follow the $1/B$ law because of the influence of the electric field quantization. However, at strong magnetic field, when the magnetic length becomes smaller than the well width, the electric quantization can be ignored, and the hybrid levels transform into the conventional Landau bulk states. From Fig. 2 we can see that the two low-field bulk SdH oscillations for the 2000-Å parabolic well are smeared out in a tilted field, which can be attributed to the hybridization of the electric and magnetic subbands.

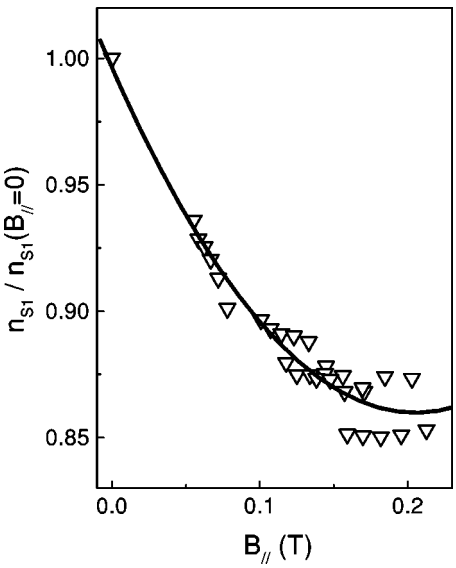

FIG. 5. Electron density of the lowest subband normalized to the density in the absence of the parallel magnetic field $B_{\|}$ as a function of $B_{\|}$ at $T=50$ mK, W=2000 Å.

For a wider 4000-Å parabolic well low-field oscillations survive in the whole tilt-angle range. This effect can also be responsible for the redistribution of the electron charge between the subbands in the tilted magnetic field. As was mentioned before, the 2D SdH oscillations are sensitive only to the normal component of the magnetic field $B_{\perp}$. Figure 1(a) shows the magnetic field dependence of the SdH oscillations at different tilt angles for sample A. In accordance with Eq. (2) the SdH oscillations are periodic in $1/B_{\perp}$, with a frequency proportional to the density in the 2D subband. Therefore by analyzing the $B_{\perp}$ position of each minimum in the magnetoresistance in a tilted field we can determine the subband density as a function of the in-plane magnetic field. In the case of two occupied subbands, the density of the lowest subband increases with parallel magnetic field. Such deviation from 2D behavior has been observed in parabolic well with two electronic subbands,[10] and has been attributed to the carrier redistribution between subbands due to the diamagnetic shift and magnetic-field-dependent effective mass.[10] Figure 5 shows the density of the 2D lowest subband as a function of the in-plane magnetic field in our wide parabolic quantum well, sample A . Surprisingly, the carrier density decreases with parallel field in contrast to the results obtained for a narrow well with two electronic subbands.[10] This reflects the fact that the system is truly self-consistent, and the changes in the electron density function profile have a noticeable effect on the potential well size and shape. The parallel magnetic field leads to a shifting of the electron wave function from the center of the well and, consequently, to a bending of the well bottom at the edge of the well. Taking into account the first-order correction to the energy we can obtain the following expression for the energy of each subband in the symmetric square quantum well:[12]

$$E(k_x,k_y)=\frac{\hbar^2k_x^2}{2m}-\alpha^{\pm}(B_{\|})k_x+\frac{\hbar^2k_y^2}{2m}+\frac{e^2B_{\|}^2\langle z^2\rangle}{2m}+E_n, \tag{5}$$

where term $(e^2B_{\|}^2\langle z^2\rangle)/(2m)$ is the diamagnetic shift in energy, for the corresponding quantum mechanical expectation $\langle z^2\rangle$ of the subband with energy E_n, $\alpha^{+}(B_{\|})>0$ for $k_x>0$, and $\alpha^{-}(B_{\|})<0$ for $k_x<0$. The term $\alpha^{\pm}(B_{\|})k_x$ leads to additional local minima at finite Fermi vector on the dispersion curve $E(k)$.[13]

Generally the diamagnetic shift may lead to a redistribution of subband densities and increase of the electron concentration of the lowest subband.[11] Because the term $\alpha^{\pm}(B_{\|})k_x$ has a sign opposite to the diamagnetic shift, it is natural to assume that it may lead to a decrease in the sheet density of the lowest subband. In contrast to the narrow parabolic well, in a wide well this mechanism can be dominant,[13] and we can see it in our experiment. It is worth noting that the periodicity of the bulk SdH oscillations is not changed with angle; therefore, the density N^{+} is constant. Because the bulk density in the well, $N_{(3D)}$, is not changed either and $N_{(3D)}=N_1^{+}+N^{+}$, we assume that $n_s=[\int z|\phi_1(z)|^2]N_1^{+}$ decreases due to the shrinking of the spatial extent of the lowest subband wave function in a parallel magnetic field. Further self-consistent calculations of the parabolic well in a parallel magnetic field will be necessary to clarify this question.

Because of the low electron density, the last peak of the bulk SdH oscillations should be observed at $B=2T$. For 2D electron gas the quantum limit should be also observed at $B>4$ T. Surprisingly we find several oscillations at higher field and quantum Hall effect plateaus with corresponding deep minima in R_{xx} at $B=8.2$ and 16.4 T. The magnetoresistance and the Hall effect data in magnetic field $B>2$ T and the Landau fan chart for the 3D and 2D subbands for sample A are shown in Fig. 6. We can see six minima after the last 3D SdH peak. We attribute such behavior to the recovery of the 2D Landau levels at higher fields. At strong magnetic field the broadening of the levels becomes B dependent.[14] The Landau level spacing increases faster with B in comparison with the level broadening ($\Gamma\sim B^{1/2}$). Therefore, the last spin-down 3D level is split into four two-dimensional Landau levels, as shown in Fig. 6(a), which leads to the recovery of the 2D Landau levels at strong field and, finally, to the formation of the quantum Hall effect in a parabolic quantum well.[15] The Landau fan chart shows that one should observe exactly six minima after the last spin-up 3D level, and the last minima correspond to the gap between the lowest and second subbands at zero magnetic field.[15] It is worth noting that the positions of the minima and maxima in a strong magnetic field do not reflect the separation of the levels but their degeneracy;[1] therefore, the positions of the gaps in the Landau fan chart do not correspond to positions of the minima in R_{xx} shown in Fig. 6(b). Observation of the quantum Hall effect in a strong magnetic field clearly demonstrates that the 2D electron system and the 3D electron gas are not spatially separated, and 3D SdH oscillations cannot be explained by the hidden disordered electron layer, as has been found in the AlInAs/InGaAs system.[16]

In the following section, we evaluate the broadening of the levels in a wide parabolic well due to the elastic scattering. All subbands overlap and therefore no 2D states should be observed in our system. We assume that other effects

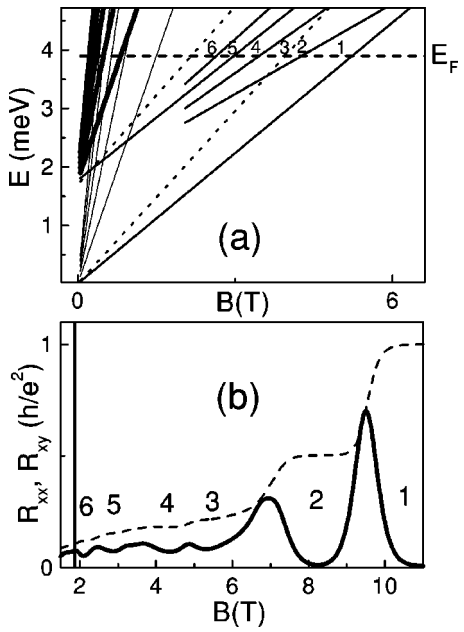

FIG. 6. (a) Energy diagram for a 2000-Å-wide quantum well. The filling factors for the corresponding minima in longitudinal resistance are indicated. Dotted lines correspond to the spin-down levels of the 2D and 3D subbands. The spin-up 3D Landau band splits into two 2D Landau levels. Dashed line, the Fermi energy at zero magnetic field. (b) Longitudinal (solid) and Hall (dashed) resistance as a function of perpendicular magnetic field at $T=50$ mK. Filling factors for corresponding minima in longitudinal resistance are indicated. Vertical line, position of the last 3D SdH peak at $B=1.9$ T (see text).

(probably screening) can be responsible for the separation of the lowest level from the highest subbands.

III. CALCULATION OF THE SCATTERING TIME AND DISCUSSION

As we already mentioned above, the three-dimensional limit may be reached by continuously increasing the width of the parabolic quantum well. The density of states of a two-dimensional system is

$$\rho_0(E)=\mathrm{Int}[E_f/(\hbar\pi^2/2mw_e^2)]^{1/2}, \tag{6}$$

where ''Int'' denotes the integer part of a number. The density of states has a step structure, which arises from the discrete energy-level spectrum. The approach of the 3D limit in the presence of the scattering is not well known. It is reasonable to suggest that the smoothing out of the steplike structures due to the broadening of the electron states is responsible for the 2D-3D transition. Elastic impurity scattering leads to the following expression for the density of states:[17]

$$\rho(E)=-\frac{2}{\pi}\sum \mathrm{Im}[G(k,E+iO)], \tag{7}$$

where $G(q,E)$ is the one-electron Green's function, which can be expressed as

$$G=\left\{E-\frac{\hbar^2k^2}{2m}+\frac{i\hbar}{2\tau}\right\}^{-1}, \tag{8}$$

where k is a wave vector and τ is the single-particle relaxation time. The thermodynamic density of states with scattering is therefore given by

$$\rho(E)=\frac{2}{\pi}\int dE'\rho_0(E')\frac{\hbar/2\tau}{(E-E')^2+(\hbar/2\tau)^2}. \tag{9}$$

Temperature broadening is very small ($\sim$0.004 meV), and we can neglect it in our calculations. It is reasonable to assume that if the elastic broadening $\hbar/2\tau$ is much larger than the energy separations between subbands, ΔE, the density of states becomes three dimensional. To evaluate the broadening in our system we calculate the single-particle relaxation time and the transport relaxation time due to the remote impurity doping and background impurities. It is worth noting that the single-particle relaxation time, or quantum time, describes the decay time of one-particle excitations and gives rise to the renormalization of the density of states in contrast to the transport relaxation time, which describes the mobility of electron gas. The transport and quantum times are obtained by numerical integration of the squared matrix elements over the allowed scattering vector using a self-consistently calculated wave function.[18] Screening of the impurity scattering potential in the presence of the 2D electron gas (2DEG), is included within the Thomas-Fermi approximation. A detailed calculation of the quantum and transport times should include different scattering mechanisms such as interface roughness scattering and alloy disorder scattering. However, our samples are overfilled and have only a 100-Å-wide spacer layer which is smaller than in the samples studied in Refs. 3–5 and therefore the remote impurity scattering should be the major scattering mechanism in this case. In addition, it is very likely that our samples have enhanced background impurity concentration in the parabolic well due to a greater reactivity of Al with oxygen. Thus we consider only two major scattering mechanisms—remote and background impurity scattering.

It is worth noting that in the multisubband systems the intersubband scattering begins to play a very important role. For a system with N subbands occupied the quantum time is given by

$$\frac{1}{\tau_i}=\sum_{j=1}^{N} P_{ij}^{(0)}, \tag{10}$$

where $P_{ij}^{(0)}$ is the transition rate for an incident electron in the i into j subband averaged over the allowed scattering vector. However, for the transport time Eq. (10) is not valid. The transport lifetime τ_t has a more complicated form and can be obtained from the Boltzmann equation, which gives[19]

$$k_i\tau_{ti}=\sum_{j=1}^{N}(K)_{ij}^{-1}k_j, \tag{11}$$

where the scattering matrix K_{ij} is defined as

TABLE I. Subband separation $\Delta_{ij}=E_j-E_i$, transport (μ_t) and quantum (μ) mobilities, and quantum level broadening $\Gamma=\hbar/2\tau$ for different subbands in a parabolic quantum well with width of 2000 Å.

Subband i	Density (10^{11} cm^{-2})	Energy (meV)	Δ_{ij} (meV)	μ_t (10^3 cm^2/V s)	μ	Γ (meV)
1	1.15	0.12	—	88	21	0.40
2	1.03	0.50	0.38	72	19	0.46
3	0.85	1.15	0.65	52	15	0.56
4	0.60	2.06	0.91	46	13	0.67
5	0.27	3.24	1.18	18	8	1.06

TABLE II. Subband separation $\Delta_{ij}=E_j-E_i$, transport (μ_t) and quantum (μ) mobilities, and quantum level broadening $\Gamma=\hbar/2\tau$ for different subbands in a parabolic quantum well with width of 4000 Å.

Subband i	Density (10^{11} cm^{-2})	Energy (meV)	Δ_{ij} (meV)	μ_t (10^3 cm^2/V s)	μ	Γ (meV)
1	0.64	0.03	—	475	170	0.05
2	0.62	0.11	0.08	203	85	0.09
3	0.57	0.25	0.14	210	56	0.14
4	0.51	0.44	0.19	119	40	0.20
5	0.43	0.70	0.25	143	34	0.22
6	0.33	1.01	0.31	76	26	0.30
7	0.22	1.38	0.37	89	26	0.30
8	0.08	1.82	0.44	13	17	0.47

$$K_{ij}=\sum_{l=1}^{N} P_{il}^{(0)}\delta_{ij}-P_{ij}^{(1)}. \tag{12}$$

The coefficient $P_{ij}^{(1)}$ is the first component of the Fourier transform of this transition rate $P_{ij}^{(0)}$. In our case we have five (eight) subbands occupied; therefore, **K** is the 5×5 (8×8) matrix. The intersubband scattering terms appear both in the diagonal and off-diagonal matrix elements. However, our system is symmetric and the intersubband scattering between subbands of different parities vanishes. We invert the matrix bf K numerically, and obtain the transport lifetime for electrons in each subband. The effective average mobility is given by

$$\mu_t=\sum_{i=1}^{N}\frac{n_i\mu_{ti}}{n_s}, \tag{13}$$

where $\mu_{ti}=(e/m)\tau_{ti}$.

We fit the calculated mobility to the measured one and obtain the background impurity concentration $N_{\rm bulk}=3\times10^{15}$ cm^{-3} for sample A. This value is higher than the expected carbon impurity contamination level in the well. For this sample, the remote impurity scattering time is calculated for $N_{\rm imp}=2\times10^{11}$ cm^{-2}. This value corresponds to the electron density in the well, $n_s\approx2N_{\rm imp}$, because Si donors from both sides of the well provide electrons to the well. For sample B we obtain $N_{\rm bulk}=1\times10^{14}$ cm^{-3}, which is in the limit of the expected carbon impurity contamination level in the well. Such a difference between samples A and B can be explained by the difference in the growth conditions. We use these values to calculate the quantum lifetime. It should be emphasized that the quantum lifetime calculated following the formalism given by Ando[18] and Gold[18] is much smaller than that measured from the amplitude of the SdH oscillations. From the fit of Eq. (2) to SdH oscillations [Fig. 1(a)] we extract the quantum time for sample A, $\tau_1=2.2\times10^{-12}$ s, which is 10 times larger than that calculated from the conventional theory for scattering in 2DEG. This discrepancy was found in GaAs/AlGaAs heterostructures[20] and was explained by a correlation correction, which suppresses the small-angle scattering. We calculate the transport and quantum lifetimes using modified theory for scattering in 2DEG with correlation corrections.[20] Tables I and II show the results of the single-particle and transport relaxation time simulations for 2000-Å and 4000-Å parabolic wells.

We can see that the transport and quantum lifetimes decrease with subband index for both structures. It is expected that the lifetime for the highest subbands can be smaller than that of the first, because the impurity scattering rate decreases very fast with momentum transfer.[18] As we have already mentioned above, from the fit of Eq. (2) to the SdH oscillations [Fig. 1(a)] we extract the quantum time τ_1 and obtain the broadening of the bottom level, $\Gamma_1=0.15$ meV, which is still smaller than the broadening calculated using the modified theory.[20,21] The measured quantum time for the 3D electron gas in sample A [Fig. 2(b)] leads to a broadening of the bulk states, $\Gamma^*=0.4$ meV. The average calculated quantum time for the four highest subbands is about 50% smaller than the measured one. It is reasonable to assume that the broadening $\Gamma_j=\hbar/2\tau_j$ should be less than half the distance between levels, $\Delta_{ij}/2$, due to the 2D confinement effect observable. Therefore, the second-level broadening for sample A, Γ_2, should be less than $\Delta_{12}/2=0.2$ meV for the two-dimensional bottom subband. For this sample, the calculated line broadening is 0.46 meV. One can argue that the higher values of the experimental quantum lifetimes can be understood assuming a lower background impurity concentration. However, in this case the level broadening for the highest subbands decreases too, and the 2D confinement effect will be observable for all subbands.

We assume that our calculations overestimate the scattering time only for the lowest levels. As has been mentioned in Ref. 20, in a well with several occupied subbands the influence of the intersubband coupling on the screening may be very pronounced. This effect may increase the quantum mobility of the lowest subbands. For example, as shown in Ref. 20 in the δ-doped 200-Å-wide AlGaAs/GaAs quantum well the quantum time in the first and second subbands was enhanced by 50% due to the occupation of the third level. Therefore, it is reasonable to attribute the reduction of the small wave vector scattering to the influence of the intersubband coupling on the screening effects. We have to note that the transport scattering time is not sensitive to this effect and is not modified by the intersubband coupling. Calculation of

the screening effects in the case of more than two subbands is a very complicated problem. We did not attempt to simulate the effect of the influence of the intersubband scattering on the screening. The qualitative behavior of the quantum and transport times is sufficient to explain the coexistence of the 2D and 3D electron gas. Assuming a 2 times enhancement of the quantum lifetime for the first and second levels due to the intersubband coupling described above, we obtain for both samples $\Gamma_2 \approx \Delta_{12}/2$, which results in the 2D confinement effect for the first subband. For the highest subbands the screening effect is less important, and the level broadening Γ_j is still larger than $\Delta_{ij}/2$; therefore, the density of states in these levels loses its 2D structure.

We have to complete this work by calculations of the level broadening for a wider parabolic quantum well. As has been mentioned above, the remote impurity scattering becomes less effective in a wide quantum well. From our calculations we find that the quantum mobility grows almost linearly for remote impurity scattering and remains constant for the background impurity scattering mechanism. We keep the impurity concentration $N_{\text{bulk}}=1\times10^{14}$ cm^{-3} for all well widths. Because the energy separation between subbands decreases with width as $\Delta_{ij}\sim W^{-2}$, we find that lowest subband will overlap with the second for a parabolic well width $W\approx7000$ Å. We assume here that the screening effect is still responsible for the 2 times overestimation of the scattering time for the first and second levels. However, we have to note that the criteria $\Gamma_j\sim\Delta_{ij}/2$ is not well defined theoretically, and further theoretical works are necessary to clarify question why the lowest subband is clearly separated in a wide parabolic well.

IV. CONCLUSIONS

The considerable attention given to the properties of wide parabolic quantum wells is in part explained by the prediction of a variety of collective phenomena such as charge-density waves and spin-density waves in dilute 3D electron systems in an intense applied magnetic field.[6] As mentioned above, the first step toward the realization of a quasi-3D free electron system has been reported in several works,[3–5] and the existence of a high-quality quasi-2D electron system with several 2D subbands has been demonstrated. In the present work we realize the system with 2D and quasi-3D electron gases coexisting in the same quantum well. We use standard analysis of SdH oscillations in the tilted magnetic field and explore the fact that 2D Landau levels are sensitive to the perpendicular magnetic field. We evaluate the broadening of the levels due to remote impurity scattering in the presence of the intersubband scattering and demonstrate that the broadening increases with subband index. The measured quantum lifetimes are qualitatively reproduced in the calculations. We find that the bottom subband does not overlap with the highest subbands. Therefore we realize a system containing 2D and 3D electron gases with almost the same Fermi energy. It is well known that some of the properties of 2D and 3D systems, such as localization in a random potential, for example, are radically different. We believe that our system can be used for the comparison of such effects in the 2D and 3D cases. We also demonstrate that the quasi-three-dimensional electron gas in quantum well with the width $W\leqslant4000$ Å is formed from four to seven highest two-dimensional subbands and has a nonuniform density profile in the z direction, in contrast to the uniform jellium systems necessary for the observation of collective phenomena. Obviously, a similar low-disordered structure with wider wells and more uniform total electron density profile is desirable for a better approximation of a 3D free-electron system.

ACKNOWLEDGMENTS

We thank G. Q. Hai for useful discussions and M. Casse for help with the dilution refrigerator. Support of this work by FAPESP, CNPq (Brazilian agencies), USP-COFECUB, and FTNS N97-1043 is acknowledged.

*Corresponding author. Electronic address: cassio@if.usp.br

[1] See, for a review, *The Quantum Hall Effect*, 2nd ed., edited by R. E. Prange and S. M. Girvin (Springer-Verlag, New York, 1990).
[2] S.S. Murzin, A.G.M. Jansen, and P.v.d. Linden, Phys. Rev. Lett. **80**, 2681 (1998).
[3] M. Shayegan, T. Sojoto, M. Santos, and C. Silvestre, Appl. Phys. Lett. **53**, 791 (1988).
[4] K. Ensslin, A. Wixforth, M. Sundaram, P.F. Hopkins, J.H. English, and A.C. Gosard, Phys. Rev. B **47**, 1366 (1992).
[5] T. Sajoto, J. Jo, L. Engel, M. Santos, and M. Shayegan, Phys. Rev. B **39**, 10 464 (1989).
[6] V. Celli and N.D. Mermin, Phys. Rev. **140**, A839 (1965); L. Brey, Phys. Rev. B **44**, 3772 (1991).
[7] W. Walukiewicz, P.F. Hopkins, M. Sundaram, and A.C. Gossard, Phys. Rev. B **44**, 10 909 (1991).
[8] T. Ando, J. Phys. Soc. Jpn. **37**, 1233 (1974).
[9] C.E. Hembree, B.A. Mason, A. Zhang, and J.A. Slinkman, Phys. Rev. B **46**, 7588 (1992).
[10] G. Salis, B. Ruhstaller, K. Ensslin, K. Campman, K. Maranovskii, and A.C. Gossard, Phys. Rev. B **58**, 1436 (1998).
[11] L. Smrecka and T. Jungwirth, J. Phys.: Condens. Matter **6**, 55 (1994).
[12] G.M. Gusev, J.R. Leite, E.B. Olshanetskii, D.K. Maude, M. Casse, J.C. Portal, N.T. Moshegov, and A.I. Toropov, Physica E **6**, 112 (2000).
[13] M.P. Stopa and S. Das Sarma, Phys. Rev. B **40**, 10 048 (1989); G.M.G. Oliveira, V.M.S. Gomes, A.S. Chaves, J.R. Leite, and J.M. Worklock, *ibid.* **35**, 2896 (1987).
[14] M.E. Raikh and T.V. Shahbazyan, Phys. Rev. B **47**, 1522 (1993).
[15] G.M. Gusev, J.R. Leite, E.B. Olshanetskii, N.T. Moshegov, A.I. Toropov, D.K. Maude, M. Casse, and J.C. Portal, Physica B **298**, 306 (2001).
[16] R.J. Nicholas, M.A. Brummell, J.C. Portal, G. Gregoris, S. Hersee, and J.P. Duchemin, Appl. Phys. Lett. **44**, 629 (1984).
[17] A. A. Abrikosov, L. P. Gorkov, and I. E. Dzyaloshinski, *Methods*

of Quantum Field Theory in Statistical Physics (Prentice-Hall, Englewood Cliffs, NJ, 1963), Sec. 39.

[18] A. Gold, Phys. Rev. B **38**, 10 798 (1988); T. Ando, J. Phys. Soc. Jpn. **51**, 461 (1982).

[19] E. Zaremba, Phys. Rev. B **45**, 14 143 (1992).

[20] P.T. Coleridge, Phys. Rev. B **44**, 3793 (1991).

[21] G-Q. Hai, N. Studart, F.M. Peeters, P.M. Koenrad, and J.H. Wolter, J. Appl. Phys. **80**, 5809 (1996).